T-Junction Grain Boundaries in Block Copolymer−Homopolymer Blends

Engin Burgaz and Samuel P. Gido*

Polymer Science and Engineering Department, Materials Research Science and Engineering Center, W. M. Keck Electron Microscopy Laboratory, University of Massachusetts, Amherst, Massachusetts 01003

Received April 26, 2000; Revised Manuscript Received September 12, 2000

ABSTRACT: T-junction grain boundaries were studied in a blend of polyisoprene homopolymer and a single graft block copolymer I_2S with two equal length blocks of polyisoprene and one arm of polystyrene linked at a common junction point. The overall polyisoprene volume fraction in the blend was 0.52, and its equilibrium morphology was lamellar. While T-junctions were previously observed to be quite rare compared to other tilt grain boundary morphologies such as chevrons and omegas, they were found in abundance in the blend used in the current study. The T-junctions in the blend show a number of distinctive characteristics including enlarged semicylindrical end caps terminating polystyrene lamella and an increase in the spacing of the lamella as they near their termination at the T-junction. Simple free energy calculations show that the homopolymer present in the blend stabilizes the cylindrical curvature of the end caps, rendering the T-junction morphology more stable in blends than in neat block copolymers. This agrees with the observed greater frequency of occurrence of the T-junctions in our blend sample than in neat block copolymers.

Introduction

Block copolymer materials that form microphase-separated morphologies such as spheres, cylinders, the cubic bicontinuous double gyroid morphology, and lamellae also form larger scale grain structures.[1,2] Defects or grain boundaries that are formed in copolymer structures are potentially important in terms of their effect on the physical properties of materials, such as mechanical, transport, and electrical properties. A relationship between melt shearing and kink band tilt grain boundary structure has been established in lamellar block copolymers.[3] The great bulk of research on block copolymer materials has been concerned with the phase transitions and the overall morphology formed. A much less investigated topic is how well ordered the morphologies are as a function of sample preparation conditions and molecular structure.[4−7] These issues are very difficult to address experimentally for several reasons: (1) quantitative measures of the degree of order, such as grain size, are difficult, and (2) when comparing the degree of order among different samples, great care must be taken to control and standardize the sample preparation conditions. Also, only a relatively small amount of theoretical work has been done to try to understand long-range order, grain structure formation, and the defects inherent in these morphologies such as grain boundaries.[8−10] Recently, defect evolution in diblock copolymer thin films was directly tracked using AFM between repeated cycles of thermal annealing.[11]

Gido and Thomas[1,2,12] classified twist and tilt grain boundaries in lamellar block copolymers, identifying two main types of twist boundaries (helicoid sections and Scherk surfaces) as well as different tilt boundary morphologies: chevron, omega, and T-junction. The boundary morphology formed was found to depend on the values of the geometrical parameters of twist and tilt which characterize the boundary. Energy calculations for different boundary morphologies under different twist and tilt geometrical conditions have been found to agree with the stability ranges for different morphologies.[8−10,12,13] In the current paper, we look in greater depth at T-junction tilt boundary morphology; the general structure of a T-junction is shown in Figure 1. At this type of tilt grain boundary, one set of lamellar planes terminates along a boundary line parallel to another set of lamellae. In the set of lamella that terminate, one type of lamella (gray in the figure) merges continuously with a layer on the opposite side of the boundary. The other type of lamella (white in the figure) terminates in a semicylindrical end cap. Depending on the material used, these end caps can be quite enlarged, with diameters larger than the white material lamellar thickness. The end cap enlargement is a focus of this study.

Here we concentrate on a blend of I_2S miktoarm star block copolymer with a homopolymer. The I_2S material is a three-arm star with two equal length arms of polyisoprene (PI) and one arm of polystyrene (PS) linked at a common junction point. The homopolymer used in the blend was low molecular weight PI. This particular blend produced a lamellar morphology with a very large concentration of T-junctions. In a total of 68 transmission electron microscope (TEM) images, each covering a $20 \times 30\ \mu$m area, 505 T-junctions were observed. By comparison, in the previous experimental study of tilt grain boundaries in neat diblock copolymers[1] T-junctions were observed quite rarely. Of 160 tilt grain boundaries measured in this previous study, only six T-junctions were observed. The difference in the frequency of observation of T-junctions between a blend of block copolymer and homopolymer and neat block copolymer is related to a stabilization of the semicylindrical end cap structure which is only possible when homopolymer is present. This lowers the energy of the T-junction structure in blends resulting in their stability even on extensive thermal annealing. The higher energy T-junctions in neat block copolymers are presumably lost due to rearrangements during annealing.

* To whom correspondence should be addressed.

10.1021/ma000729s CCC: $19.00
Published on Web 10/21/2000

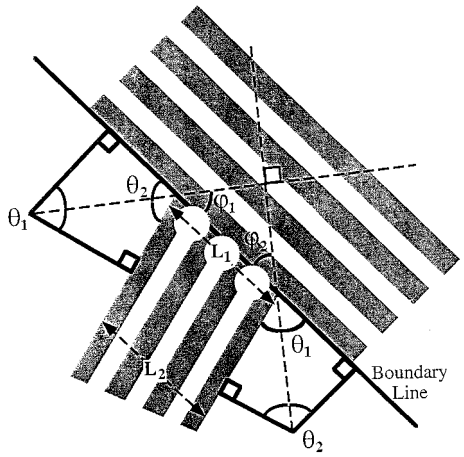

Figure 1. T-junction grain boundary geometry. Measurement of tilt angles, θ_1 and θ_2, and asymmetry angles, φ_1 and φ_2, are shown.

The geometry of a T-junction is illustrated in Figure 1. The tilt, θ, of the boundary is the angle between the normals to the two sets of lamella, in the two grains on either side of the boundary. As shown in the figure, θ can be measured in two ways which gives two supplementary angles θ_1 and θ_2. The smaller of the two tilt angles is θ_1 and will be used in this paper as the measure of tilt. When we refer to *tilt angle* or θ, we are referring to θ_1. A symmetry plane for the grain boundary bisects each θ_i. In pure chevron and omega boundary geometries, the grain boundary resides at this plane of symmetry.[1] However, as shown in the figure, the plane of the boundary can deviate by an angle φ from the symmetry plane. Two ways of measuring φ are possible, corresponding to the two ways of measuring tilt. We will use φ_1 as a measure of boundary asymmetry and will refer to it as φ; the angles φ_1 and φ_2 are complementary. Finally, as illustrated in the figure, the tilt angles θ_i also directly give the angles that the lamella on the left-hand side make when they impinge on the lamella on the right. The smaller way of measuring this angle is the same as θ_1. If θ_1 and φ_1 are 90° and 45°, respectively, the boundary has pure T-junction geometry.[1] All T-junctions must satisfy the geometrical relationship $\theta_i + 2\varphi_i = 180°$, where i is either 1 or 2.

Experimental Section

The I_2S miktoarm star copolymer used in this study is the same material as sample I_2S-3 in ref 14. The synthesis and molecular characterization are given in this previous publication. The number-average molecular weights of the PS arm, a single PI arm, and the total molecule are 61 200, 14 800, and 83 000 g/mol, respectively. The PI volume fraction is 0.38, and the polydispersity is 1.04. A blend of this block copolymer with low molecular weight (1200 g/mol) PI homopolymer was prepared by casting from a common solution in toluene such that the overall PI volume fraction was increased to 0.52.

The blend was slowly cast over 7 days from 5 vol % solutions in toluene, a nonpreferential solvent, forming a solid film 2 mm thick. The solid film was let stand under high vacuum for 5 more days at room temperature in order to completely remove residual solvent. It was then annealed for 1 week in a vacuum oven at 120 °C in order to further promote the formation of well-ordered structures. After annealing, samples for electron microscopy were microtomed in a Leica Ultracut cryoultramicrotome. Sections approximately 50−100 nm thick were cut with a Diatome diamond knife at a sample temperature of −110 °C and a knife temperature of −90 °C. The sections were stained with OsO_4 for 4 h, which oxidizes the double bonds of the PI, rendering it dark relative to the PS in TEM micrographs. TEM imaging was performed on a JEOL 100 CX operated at 100 kV accelerating voltage.

TEM images of the samples containing T-junction grain boundaries were recorded. Enlarged photographic prints of these images were made, and from these prints morphological observations and geometrical measurements of boundary parameters were made. The true boundary angles can only be directly measured from the TEM image if the electron beam projection direction is simultaneously perpendicular to the lamellar normals on both sides of the boundary. When the projection direction is perpendicular to the normals of a set of lamellae (i.e., projection parallel to the lamellar planes), the banded image observed in TEM is very sharp and the spacing of the banding is the true lamellar spacing. The true lamellar spacing for these materials is known from SAXS. The true lamellar spacing from TEM imaging on OsO_4 stained samples may differ by a few percent from that obtained by SAXS due to the effect of the stain. However, these differences introduce less error than other aspects of the geometrical analysis. If the lamellar orientation changes such that the electron beam is no longer parallel to the planes, the observed lamellar spacing will change, and the contrast between light and dark layers will be reduced. Tilting the thin sample film so that it is no longer perpendicular to the electron beam also changes both the spacing and contrast of the projection of the lamellar layers. A detailed analysis of these geometrical effects on the spacing and contrast of projected lamellar images was given by Gido and Thomas[1,2] in their previous work on lamellar grain boundaries. In general, by knowing the sample thickness, the goniometer tilt of the sample in the TEM, and the true lamellar spacing and measuring angles and projected lamellar repeats from the image, one can calculate the true boundary geometry.

In the present study, we either analyzed boundaries which, by chance, were already at or near the correct orientation for direct determination of tilt geometry or we tilted the samples in the TEM in order to achieve this geometry. The uncertainty inherent in these procedures and measurements is reflected in the fact that data are reported as averages for 5° ranges of tilt.

Results

In 68 micrographs of the I_2S−homopolymer blend, a total of 505 T-junctions were identified and analyzed. Figure 2 shows a TEM image of the blend with a number of T-junctions that illustrate some general observations about these structures: (1) the PI material is always continuous across the boundary, and (2) the PS lamella that terminate at the boundary do so in semicylindrical end caps which are enlarged relative to the PS lamellar thickness. (3) Often there appears to be an increase in the lamellar repeat distance as the lamellar layers that terminate approach the boundary. This spreading is most prominent when the boundaries approach the pure T-junction geometry ($\theta = 90°$ and $\varphi = 45°$), as in the regions labeled *A* in Figure 2. (4) The T-junction boundaries in the blend are generally fragmented into a number of smaller boundary segments.

The degree of lamellar spreading in T-junctions was measured for all the boundaries we observed by a method illustrated with Figure 1. A distance, L_1, was measured parallel to the grain boundary plane across the widest points of a number of the enlarged PS end caps. A second measurement, L_2, was taken parallel to the boundary plane and to L_1 far from the boundary where the lamellar repeat distance is unaffected by the boundary. L_2 was measured over the same number of lamellar repeats as was used for L_1. The ratio L_1/L_2 then characterizes the spreading of the lamellar layers at the T-junction. Figure 3 shows a histogram of number of

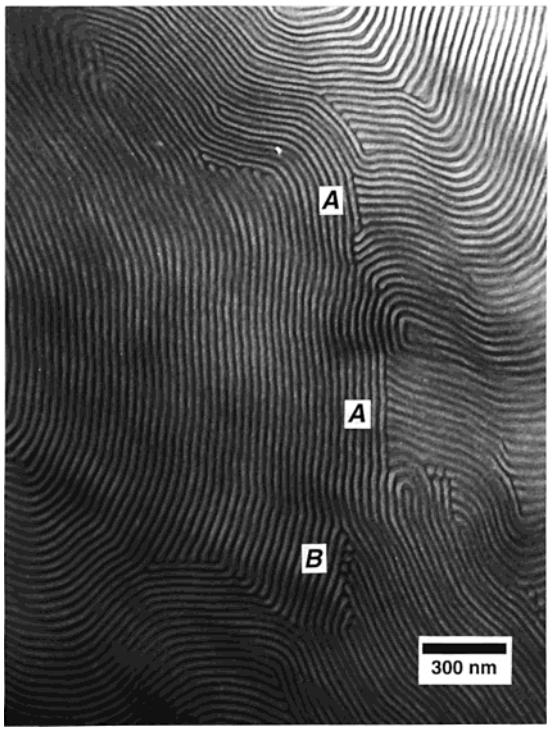

Figure 2. TEM micrograph of the I_2S−hPI blend containing T-junction grain boundaries: (A) regions with approximately pure T-junction geometry; (B) regions with cylindrical domains segregated at the grain boundary.

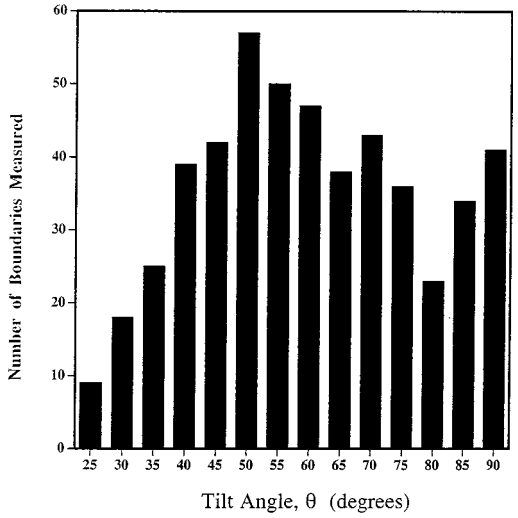

Figure 3. Number of T-junction grain boundaries observed and measured as a function of tilt angle. Data are grouped into 5° tilt ranges which are labeled by the highest angle in each range.

boundaries observed and measured as a function of tilt angle, θ. The boundaries are grouped together in 5° tilt angle ranges which are identified by the high angle in the range. For instance, boundaries with tilt angles greater than 55° up to and including 60° are included in the grouping reported at 60°. The concentration of boundaries appears to have a maximum in the 45°−50° tilt range. Figure 4 shows a plot of φ vs θ for all the boundaries measured in this study. The data points are clustered around a line representing the condition $\theta + 2\varphi = 180°$, which characterizes the T-junction geometry. This confirmation that the grain boundaries in our data set conform to the geometrical definition of the T-junction validates the methods used to measure boundary tilt and asymmetry angles from TEM images. Figure 5 is a plot of the lamellar expansion factor L_1/L_2 vs tilt angle. The data points represent averages over all the boundaries in each of the same 5° tilt ranges used in the histogram (Figure 3), and the error bars indicate one standard deviation. The expansion factor increases with increasing tilt angle up to 90°. There appears to be a preference for a negative expansion factor (a compression of the lamellar layers) for tilt angles smaller than about 40°. However, the smaller number of boundaries measured at these small angles and the fact that noncompressed boundary geometries are within the range of experimental data scatter makes this conclusion somewhat tentative. On the other hand, there is a clear and statistically relevant tendency for positive expansion for higher tilt angles, especially as pure T-junction geometry ($\theta = 90°$) is approached. The spreading of the lamellar layers as they approach the T-junction boundary occurs over a distance equal to between one and two lamellar long periods.

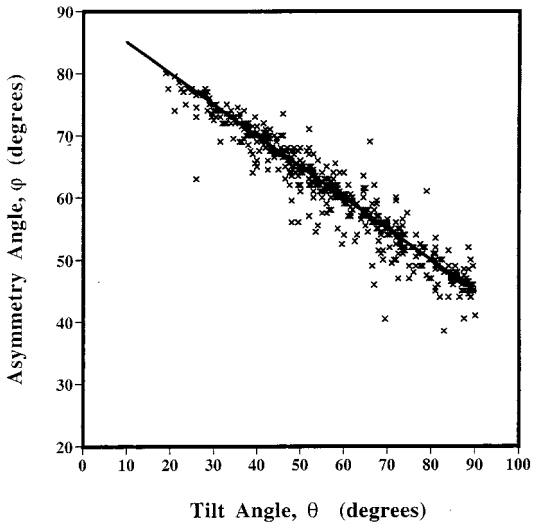

Figure 4. Plot of asymmetry angle vs tilt angle for all the T-junctions measured in the I_2S−hPI blend. The data are clustered around a line representing the T-junction geometrical condition: $\theta + 2\varphi = 180°$.

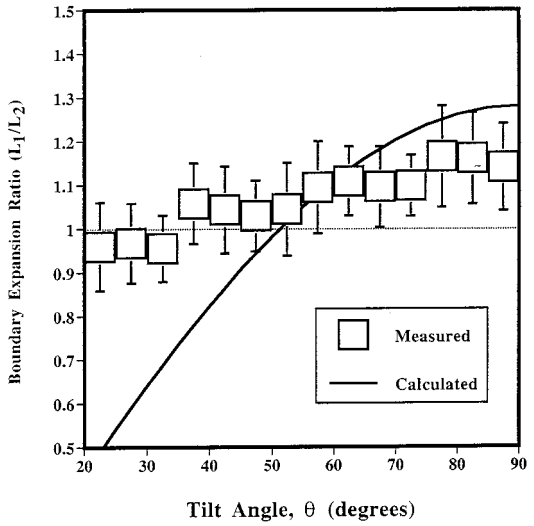

Figure 5. T-junction boundary expansion ratio as a function of tilt angle. The square symbols represent averages over all the boundaries in each 5° tilt range. The error bars represent one standard deviation. The solid curve is the expansion factor calculated using the simple model shown in Figure 8.

Discussion

We now will endeavor to explain the trends observed in the experimental data using geometrical arguments as well as some simple free energy calculations. Although the models used to carry out these calculations are rough, they provide insight into the relevant physics and they predict the correct trends. Clearly, the lamellar domains of one of the component materials must terminate in some sort of cap at the T-junction boundary. The end caps are observed to form an approximately semicylindrical geometry as one would expect since a cylinder is a surface of constant mean curvature which minimizes the interfacial area between the two components.[15] The semicylindrical end cap may have a diameter that is enlarged relative to the PS lamellar domain thickness.

The tendency for the end cap to become enlarged is simple to understand. At close to 50/50 volume fractions the block copolymer−homopolymer blend used in this study wants to form the flat interfaces of the lamellar morphology. However, the external constraint imposed by the boundary forces the material to curve into a cylindrical geometry. One can easily calculate the radius that minimizes the energy of this lamellar forming material when it is constrained to form a cylinder. This calculation is performed using the mean field, wedge free energy of Milner,[16,17] and the assumption of incompressibility, by minimizing with respect to cylinder radius. An additional term is added to the free energy to account for the mixing of PI homopolymer with the I_2S PI blocks. This term is of the type used by Leiber, Orland, and Wheeler[18] and assumes that the low molecular weight homopolymer is evenly distributed throughout the microphase-separated PI domains. Equation 1 is the free energy, in kT units, associated with a single block copolymer molecule plus the average number of homopolymer chains in the system per block copolymer molecule. The first and second terms represent the chain stretching energies of the A and B blocks, respectively. For i equal to A or B, the domain brush heights are h_i, the degrees of polymerization for a single arm are N_i, the Kuhn lengths are b_i, and the number of arms of each material per block copolymer molecule are n_i. The mean curvature, H, of the interfacial surface is zero in the lamellar morphology and is equal to $1/(2h_i)$ in the cylinder morphology, where i is the component in the core of the cylinders and thus h_i is the cylinder radius. When applied to cylinders, the free energy in eq 1 is formulated for the A block in the cylinder core. The third term in eq 1 is the interfacial energy where γ is the interfacial energy per unit area and σ is the grafting density of the block copolymer chains at the interface. The final term is the combinatorial entropy of mixing of the homopolymer chains in the domains of the same type. As written in eq 1, B homopolymer is mixed into the B domains. In this term N_h is the degree of polymerization of the homopolymer, n_h is the number of homopolymer chains per block copolymer, and η is the volume fraction of homopolymer in the overall B domains. In these calculations the following values, obtained from the literature,[19] were used for various system parameters: $\nu_I = 132$ Å^3, $\nu_S = 176$ Å^3, $b_I = 6.8$ Å, and $b_S = 6.9$ Å, where ν_i are segmental volumes and b_i are Kuhn lengths. The interfacial energy at the annealing temperature of 120 °C, $\gamma = 0.014$ kT/Å^2, was calculated using the expression of Helfand and Tagami[20] with the experimentally determined χ of Mori et al.[21]

$$\frac{f}{kT} = \frac{n_A \pi^2 h_A^2}{16 N_A b_A^2} \frac{1 - \frac{3}{2} H h_A}{1 - H h_A} + \frac{n_B \pi^2 h_B^2}{16 N_B b_B^2} \frac{1 + \frac{3}{2} H h_B}{1 + H h_B} + \frac{\gamma}{\sigma} + \frac{n_B N_B + n_h N_h}{N_h} \eta \ln \eta \quad (1)$$

The results of these calculations are given in Table 1, which lists calculated PS brush height (h_S), calculated PI brush height (h_I), total block copolymer layer thickness ($h_T = h_S + h_I$), and free energy per unit volume. Domain geometries and free energies were calculated for both the equilibrium lamellar morphology and the lowest energy constrained cylinder morphology. In the lamellar geometry h_T is half of the long period, while in the cylindrical geometry h_T is the cylinder radius, including both the core and corona layers. For the I_2S−hPI blend, a number of different cases were considered: (1) Calculation of the equilibrium lamellar geometry and free energy in the I_2S−hPI blend where the hPI concentration in the PI lamellar domains is determined by its overall concentration in the blend. (2) Cylinders with PS in the core and PI in the corona. The concentration of hPI in the PI domains is determined by the overall hPI concentration in the blend. (3) Cylinders with PS in the core and PI in the corona in which the hPI concentration in the PI domains is allowed to vary. The results reported were obtained by minimizing the free energy with respect to the hPI concentration in the cylindrical corona. This corresponds to a situation that actually occurs in the blends, where the formation of cylindrical end caps generates a free energy driving force to pull hPI preferentially into the PI domains around these end caps, thus stabilizing the cylindrical structures. (4) Inverted cylindrical structures with PI in the core and PS in the corona. The concentration of hPI in the core domains is determined by the overall hPI concentration in the blend. (5) Inverted cylindrical morphology with PI in the core and PS in the corona in which the hPI concentration in the core is allowed to vary in order to minimize free energy. Cases 4 and 5 were not observed experimentally, and the calculations were done in order to understand this fact.

For all cases considered, the radius of the lowest energy cylinder geometry (h_T) is larger than the lamellar layer thickness. Thus, if cylinder end caps must be formed, there will be an energetic driving force to enlarge them. The calculations for the I_2S−hPI blend clearly show that the free energy is significantly lower for cylindrical end cap geometries that place PS in the core and PI in the corona (cases 2 and 3) than for the inverted structures (cases 4 and 5). This explains why the end caps always form with PS on the inside and agrees with the general trend observed in studies of miktoarm star morphology[14,16,17,22,23] where multiple arms of the same type prefer to be on the convex side of a curved interface in order to reduce crowding. Henceforth, we will only consider case 2 and 3 cylindrical end caps with PS cores. One would expect the free energy per chain in the best possible cylinder to be higher than the energy in the equilibrium lamellar structure. This is the situation for blends where the hPI concentration in the PI corona is fixed at that determined by the average in the blend, case 1. The overall PI volume fraction in the blend is 0.52, and this corresponds to a hPI volume fraction within the PI domains of 0.49, or

Table 1. Calculated Domain Sizes and Free Energies

material	morphology[a]	cylinder core material[b]	ϕ_{PI}	h_S (Å)	h_I (Å)	h_T (Å)	h_T(C)/h_T(L)	free energy (kT/nm^3)
I_2S/hPI blend (case 1)	L		0.52	164	178	341		−24.824
I_2S/hPI blend (case 2)	C	S	0.52	307	136	444	1.30	−24.823
I_2S/hPI blend (case 3)	C	S	0.53	299	138	437	1.28	−24.864
I_2S/hPI blend (case 4)	C	I	0.52	245	213	458	1.34	−17.161
I_2S/hPI blend (case 5)	C	I	0.44	210	238	448	1.31	−20.055

[a] Morphology: L = lamella, C = cylinders. [b] Cylinder core material: S = polystyrene, I = polyisoprene.

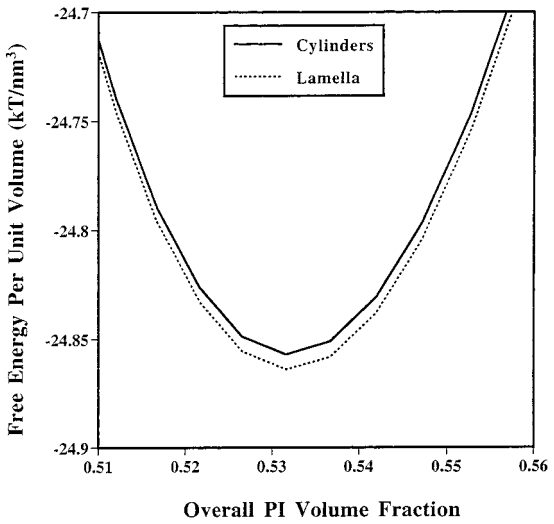

Figure 6. Free energy per nm^3 as a function of the overall PI volume fraction in the I_2S−hPI blend. Energies are plotted for both lamellar and cylindrical geometries.

about 23 low molecular weight hPI chains per I_2S block copolymer molecule.

Figure 6 shows the free energy per unit volume for both optimized cylinders and lamella plotted against total PI volume fraction over a limited volume fraction range containing both the overall blend composition (ϕ_{PI} = 0.52) and the minima of the two free energy curves (about ϕ_{PI} = 0.53). Although the energy in the lamellar morphology is lower than that in the cylinder morphology at every composition, the optimum cylinder energy at ϕ_{PS} = 0.53 is actually lower than the lamellar energy at the overall composition of the blend. The free energy curves rule out the possibility of an equilibrium coexistence between lamellar and cylindrical morphologies in this blend system. However, if an additional constraint, the existence of a grain boundary in this case, forces the formation of cylindrically curved interface, then it is clear that this cylindrical structure will be stabilized by drawing in additional hPI in excess of its overall concentration in the blend. The volume of material involved in T-junctions in the sample is vanishingly small compared to the total sample volume, and thus the slightly increased concentration of hPI at the T-junctions will have essentially no effect on the overall hPI concentration elsewhere in the blend. We believe that it is this ability to stabilize the semicylindrical end caps with excess homopolymer that underlies their frequent occurrence in the I_2S−hPI blend. This stabilization is not possible in the neat diblock copolymers of the previous study,[1] thus explaining the relative rarity of T-junctions in these systems.

Although lamellar and cylindrical morphologies cannot co-exist in our I_2S−hPI blend system at equilibrium, grain boundaries are nonequilibrium defect structures which must be analyzed as constrained local free energy

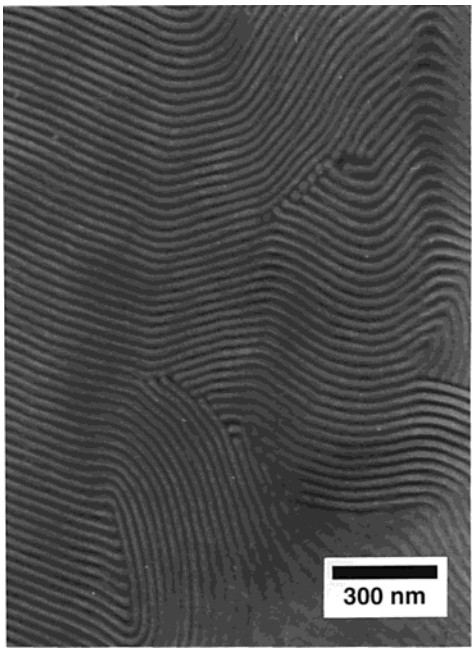

Figure 7. TEM micrograph of a T-junction in the I_2S−hPI blend with cylinders isolated in the grain boundary.

minima. Under the constraints of grain boundary geometry our calculations show that cylinders will pull in excess homopolymer, lowering their free energy below that of the lamella where the homopolymer concentration is unchanged from its bulk value. These calculations indicate that it could be possible for cylindrical domains to cluster at a T-junction grain boundary. This is in fact observed, as shown in the areas labeled B in Figure 2 as well as in Figure 7, with the I_2S−hPI blend materials. Although not as common as T-junctions with simple semicylindrical end caps, grain boundaries are frequently observed in these systems with cylinders concentrated at the boundary. The observation of cylinders at the T-junction boundaries is strong evidence for the segregation of excess homopolymer since these full cylinders are not stable at the bulk homopolymer concentration of the sample. Preferential segregation of minor components, such as impurities, to grain boundaries is commonly observed in other materials such as metals. The composition difference in the grain boundary region often leads to the formation of a different phase in the boundary region, analogous to our observation of cylinders at the boundary.[24] The fact that such cylinder containing T-junctions were not observed in the previous study[1] is a result of the fact that this study used pure block copolymers rather than blends.

Using the constrained cylinder radius for the optimized blend (case 3) reported in Table 1, we can make a very rough calculation of the amount of lamellar spacing expansion at the T-junction. This calculation uses the geometrical model shown in Figure 8. On the basis of this model, the expansion factor L_1/L_2 should

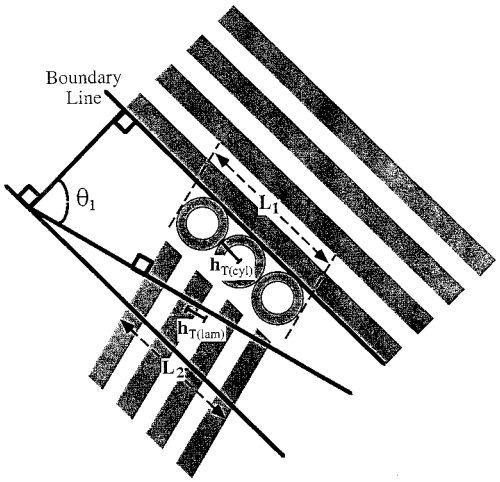

Figure 8. Simple geometrical model for the expansion of the layer spacing at a T-junction. The semicylindrical end cap spacing at the boundary line is approximated by packing constrained cylinders of the optimal diameter side-by-side. The spacing of these cylinders (L_1) is to be compared with the spacing of unperturbed lamella away from the boundary line (L_2).

be given as $\{h_T(C)/h_T(L)\}$ sin θ. These values provide the curved line in Figure 5. At a tilt angle of about 51°, the simple geometry in Figure 8 indicates that the expansion due to the cylindrical caps is exactly compensated by the foreshortening effect of the projection of the grain boundary line onto the lamellar normal direction. At this condition the end caps nest easily into one another, and no expansion of the lamellar spacing is required. This convenient geometry for avoiding expansion of the lamella from their equilibrium spacing as they approach the end caps may underlie our observation of the largest number of T-junction boundaries around 50° tilt. The geometry of Figure 8 also indicates that for tilt angles below 51° that the lamellar spacing actually must be compressed as the end caps are approached. This energetically unfavorable situation may explain why we observed comparatively few T-junctions in this lower tilt angle range.

The simple calculation of Figure 8 clearly overestimates both layer expansion at high tilt angles and layer compression at low tilt angles. The cylinders placed side-by-side at the boundary in Figure 8 do not conserve volume. Voids are created between adjacent cylinders and the boundary line. Filling these voids necessitates a smaller degree of expansion, more in line with experimental observation. The T-junctions have a way of avoiding energetically costly compression of the lamellar layers at low tilt angles. As shown in the TEM micrograph of Figure 9, the lamella of low tilt angle T-junctions often turn as they approach the boundary line, producing a local increase in tilt angle which reduces compression. This compound tilt boundary is actually a chevron beside a T-junction.

The expansion of the lamellar layers as they approach the cylindrical caps at the T-junction causes a packing problem for the lamellar layers. The accumulated expansion of a number of adjacent lamella begins to move the layers badly out of registry with the bulk. We believe that this observation may underlie the fragmented nature of most T-junctions observed in the I_2S−hPI blend. By fragmenting, the T-junctions avoid adding together the expansion effects of too many adjacent layers. Generally, the fragmented blocks of T-junction

Figure 9. TEM micrograph of a low tilt angle T-junction in the I_2S−hPI blend in which the lamella bend to increase the local tilt angle right before terminating at the boundary line. This is essentially a compound tilt angle with both T-junction and chevron components.

boundary observed in this study contained between 5 and 10 lamellar repeats. This size appears to remain nearly constant across the range of tilt angles observed. The expansion at the semicylindrical end caps is much less pronounced in neat diblock T-junctions, thus allowing long T-junction boundaries.[1]

Conclusions

The presence of homopolymer in a blend with a block copolymer stabilizes the formation of enlarged, semicylindrical end caps in T-junction tilt grain boundaries. This stabilization, which is not possible in a neat block copolymer, underlies the significant difference in the frequency with which T-junctions are observed in the blend and in neat block copolymers: Over 500 T-junctions were observed in 68 TEM images in the blend while T-junctions are very rare in neat block copolymers. The enlargement of the semicylindrical end caps relative to the thickness of the lamellar layers that they terminate is driven by a free energy reduction. Difficulty in packing these enlarged end caps side-by-side along the T-junction grain boundary leads to the spreading of the lamellar layers on one side of the boundary. This spreading, in turn, drives a preference for fragmented rather than continuous T-junctions in the blend material. Although the current study was conducted on a blend of homopolymer with an I_2S miktoarm star block copolymer, the stabilizing effect of homopolymer on semicylindrical end caps in T-junctions is most likely a general effect. The effects of this stabilization (enlarged end caps and a high concentration of T-junctions) should be found in blends of homopolymer and block copolymers of other architectures such as diblocks and triblocks.

Acknowledgment. The blend samples used in this study were prepared by K. Laverdure. The block copolymers were synthesized by S. Pispas and J. W. Mays as part of a previous study. Funding for this research

was provided by the U.S. Army Research Office under Contracts DAAG55-98-1-0116 and DAAG55-98-1-0005. Central Facility support from the Materials Research Science and Engineering Center (MRSEC) at the University of Massachusetts−Amherst as well as the W. M. Keck Electron Microscopy Laboratory is also acknowledged.

References and Notes

(1) Gido, S. P.; Thomas, E. L. *Macromolecules* **1994**, *27*, 6137.
(2) Gido, S. P.; Gunther, J.; Thomas, E. L.; Hoffman, D. *Macromolecules* **1993**, *26*, 4506.
(3) Polis, D. L.; Winey, K. I. *Macromolecules* **1996**, *29*, 8180.
(4) Beyer, F. L.; Gido, S. P.; Bueshl, C.; Iatrou, H.; Uhrig, D.; Mays, J. W.; Chang, M. Y.; Garetz, B. A.; Balsara, N. P.; Beck Tan, N.; Hadjichristidis, N. *Macromolecules* **2000**, *33*, 2039.
(5) Newstein, M. C.; Garetz, B. A.; Balsara, N. P.; Chang, M. Y.; Dai, H. J. *Macromolecules* **1998**, *31*, 64.
(6) Dai, H. J.; Balsara, N. P.; Garetz, B. A.; Newstein, M. C. *Phys. Rev. Lett.* **1996**, *77*, 3677.
(7) Garetz, B. A.; Balsara, N. P.; Dai, H. J.; Wang, Z.; Newstein, M. C.; Majumdar, B. *Macromolecules* **1996**, *29*, 4675.
(8) Matsen, M. W. *J. Chem. Phys.* **1997**, *107*, 8110.
(9) Netz, R. R.; Andelman, D.; Schick, M. *Phys. Rev. Lett.* **1997**, *79*, 1058.
(10) Villain-Guillot, S.; Netz, R. R.; Andelman, D.; Schick, M. *Physica A* **1998**, *249*, 285.
(11) Hahm, J.; Lopes, W. A.; Jaeger, H. M.; Sibener, S. J. *J. Chem. Phys.* **1998**, *109*, 10111.
(12) Gido, S. P.; Thomas, E. L. *Macromolecules* **1994**, *27*, 849.
(13) Gido, S. P.; Thomas, E. L. *Macromolecules* **1997**, *30*, 3739.
(14) Pochan, D. J.; Gido, S. P.; Pispas, S.; Mays, J. W.; Ryan, A. J.; Fairclough, J. P. A.; Hamley, I. W.; Terrill, N. J. *Macromolecules* **1996**, *29*, 5091.
(15) Thomas, E. L.; Anderson, D. M.; Henkee, C. S.; Hoffman, D. *Nature* **1988**, *334*, 598.
(16) Milner, S. T. *Macromolecules* **1994**, *27*, 2333.
(17) Gido, S. P.; Wang, Z.-G. *Macromolecules* **1997**, *30*, 6771.
(18) Leibler, L.; Orland, H.; Wheeler, J. C. *J. Chem. Phys.* **1983**, *79*, 3550.
(19) Brandrup, J.; Immergut, E. H. *Polymer Handbook*, 2nd ed.; Wiley: New York, 1975.
(20) Helfand, E.; Tagami, Y. *J. Chem. Phys.* **1972**, *56*, 3592.
(21) Mori, K.; Hasegawa, H.; Hashimoto, T. *Polym. J.* **1985**, *17*, 799.
(22) Lee, C.; Gido, S. P.; Poulos, Y.; Hadjichristidis, N.; Beck Tan, N.; Trevino, S. F.; Mays, J. W. *J. Chem. Phys.* **1997**, *107*, 6460.
(23) Tselikas, Y.; Iatrou, H.; Hadjichristidis, N.; Liang, K. S.; Mohanty, K.; Lohse, D. J. *J. Chem. Phys.* **1996**, *105*, 2456.
(24) Hu, H. *The Nature and Behavior of Grain Boundaries*; Plenum Press: New York, 1972.

MA000729S